Ultrasonic study of the charge mismatch effect in charge-ordered $(Nd_{0.75}Na_{0.25})_x(Nd_{0.5}Ca_{0.5})_{1-x}MnO_3$

2006 J. Phys.: Condens. Matter 18 8563

(http://iopscience.iop.org/0953-8984/18/37/014)

INSTITUTE OF PHYSICS PUBLISHING JOURNAL OF PHYSICS: CONDENSED MATTER

J. Phys.: Condens. Matter **18** (2006) 8563–8571 doi:10.1088/0953-8984/18/37/014

Ultrasonic study of the charge mismatch effect in charge-ordered $(Nd_{0.75}Na_{0.25})_x(Nd_{0.5}Ca_{0.5})_{1-x}MnO_3$

Liang Jiang, Jinrui Su, Hui Kong, Yi Liu, Shiyuan Zheng and Changfei Zhu[1]

Laboratory of Advanced Functional Materials and Devices, Department of Materials Science and Engineering, University of Science and Technology of China, Hefei 230026, People's Republic of China

E-mail: cfzhu@ustc.edu.cn

Received 7 March 2006, in final form 20 July 2006
Published 1 September 2006
Online at stacks.iop.org/JPhysCM/18/8563

Abstract

The resistivity, magnetization and ultrasonic properties of charge-ordered polycrystalline $(Nd_{0.75}Na_{0.25})_x(Nd_{0.5}Ca_{0.5})_{1-x}MnO_3$ have been investigated from 50 to 300 K. A considerable velocity softening accompanied by an attenuation peak was observed around the charge-ordering transition temperature (T_{CO}) upon cooling. The simultaneous occurrence of the charge ordering (CO) and the ultrasonic anomaly implies strong electron–phonon coupling, which originates from the cooperative Jahn–Teller effect. At very low temperature, another broad attenuation peak was observed, which is attributed to the phase separation (PS) and gives a direct evidence of spin–phonon coupling in the compound. With increasing x, T_{CO} shifts to lower temperature, the magnetization of the system is strengthened and the PS is enhanced. The temperature dependence of the longitudinal modulus shows that the Jahn–Teller coupling energy E_{JT} decreases with increasing Na content. The analysis suggests that the charge mismatch effect may be the main reason for the suppression of the CO and enhancement of the PS.

1. Introduction

Hole-doped perovskite manganites $Ln_{1-x}A_xMnO_3$ (Ln: trivalent rare-earth ions, A: divalent alkaline-earth ions) have attracted much attention because of their special structural, magnetic, and electronic properties as well as the potential applications in magnetic devices and sensors [1–4]. Besides the well-known negative colossal magnetoresistance (CMR) effect near the Curie temperature, another interesting phenomenon that has been widely studied recently is the real-space ordering of charge carriers. Among the charge-ordered systems, the half-doped system in which the ratio of Mn^{3+} to Mn^{4+} is 1:1 has attracted great interest due to the

[1] Author to whom any correspondence should be addressed.

particular magnetic and electronic states. The stability of the charge-ordered state can be greatly modified by the average radius of the A-site cations $\langle r_A \rangle$ [5]. For instance, $Nd_{0.5}Ca_{0.5}MnO_3$ with small $\langle r_A \rangle$ (1.17 Å) displays a CO transition near 250 K and shows no ferromagnetism at any temperature [6], while $La_{0.5}Ca_{0.5}MnO_3$ ($\langle r_A \rangle = 1.20$ Å) shows a complex magnetic transition and weaker charge-ordering effect [7]. Rodriguez-Martinez [8] and Terai [9] found that the size variance σ^2 defined by the equation $\sigma^2 = \Sigma y_i r_i^2 - \langle r_A \rangle^2$, where y_i is the fractional occupancy of A-site ions, r_i is the corresponding ionic radius, can also affect the electronic and magnetic properties of charge-ordered manganites [9].

In contrast to systems substituted with alkaline-earth cations, there are few reports on the less commonly studied systems with alkaline ions [10–14]. For the manganites doped with alkaline ions, the ratio of Mn^{3+} to Mn^{4+} is also 1:1 when the doping level is 0.25. We speculate that the CO phenomenon also exists in systems with small $\langle r_A \rangle$. However, $La_{0.75}Na_{0.25}MnO_3$, whose $\langle r_A \rangle$ (1.22 Å) is smaller than that of $Nd_{0.5}Sr_{0.5}MnO_3$ ($\langle r_A \rangle = 1.24$ Å), a typical CO system, does not show a CO transition and has a high Curie temperature T_C and large CMR effect near room temperature [14, 15]. Ye attributed this anomaly to the charge mismatch effect [14]. Recently, Jirák and Liu observed the CO phenomenon in $Pr_{0.75}Na_{0.25}MnO_3$ and $Nd_{0.75}Na_{0.25}MnO_3$ through neutron diffraction and magnetic measurements [16, 17]. $Nd_{0.75}Na_{0.25}MnO_3$ has similar $\langle r_A \rangle$ (1.18 Å) to $Nd_{0.5}Ca_{0.5}MnO_3$, while the T_{CO} (about 180 K) is much lower than that of $Nd_{0.5}Ca_{0.5}MnO_3$ (250 K) [17]. So $(Nd_{0.75}Na_{0.25})_x(Nd_{0.5}Ca_{0.5})_{1-x}MnO_3$ is a good system for investigating the difference between the alkaline-earth metal doping and the alkaline metal doping, for this doping does not significantly change the $\langle r_A \rangle$ and the ratio of Mn^{3+} to Mn^{4+}.

As a sensitive tool, the ultrasonic technique has proven to be successful for studying electron–phonon and spin–phonon couplings in perovskite materials. It has been found that around T_{CO}, the abnormal change of velocity and attenuation is closely related to the strong electron–phonon coupling [18–20]. In this paper, we present the ultrasonic velocity and transport studies on the charge-ordered $(Nd_{0.75}Na_{0.25})_x(Nd_{0.5}Ca_{0.5})_{1-x}MnO_3$ in order to obtain more information about the alkaline metal doping effects on the charge-ordered manganites.

2. Experiments

The polycrystalline samples of $(Nd_{0.75}Na_{0.25})_x(Nd_{0.5}Ca_{0.5})_{1-x}MnO_3$ ($x = 0, 0.25, 0.5, 0.75, 1$) were synthesized via a conventional solid-state reaction method. A stoichiometric mixture of high-purity Nd_2O_3 (preheated at 1000 °C for 10 h), $CaCO_3$, Na_2CO_3, and MnO_2 was well ground and calcined at 1000, 1100, and 1150 °C in air for 12 h. Finally, the obtained powder was pressed into pellets and sintered in air for 12 h at different temperatures depending on the sodium content (1200 °C for $x = 1$, 1250 °C for $x = 0.75$ and $x = 0.5$, 1300 °C for $x = 0.25$ and $x = 0$), and furnace cooled to room temperature at the rate of 1.5 K min^{-1}.

The crystal structure of the samples was determined by powder x-ray diffraction on a powder x-ray diffractometer (Japan Rigaku MAX-RD) using Cu Kα radiation ($\lambda = 1.5418$ Å) at room temperature. The electrical resistance of the sample was measured as a function of temperature by the standard four-terminal configuration. Magnetization $M(T)$ measurements were performed on bulk samples using a superconducting quantum interference device (SQUID) magnetometer from Quantum Design (MPM-5).

The ultrasonic velocity and attenuation measurements were performed on a Matec-7700 oscillator/receiver series with a conventional pulsed-echo-overlap technique. Longitudinal ultrasonic wave pulses are generated by a X-cut quartz transducer at a frequency of 10 MHz. The relative change of sound velocity $\Delta V/V$ was defined as

$$\Delta V/V = (V - V_{min})/V_{min}$$

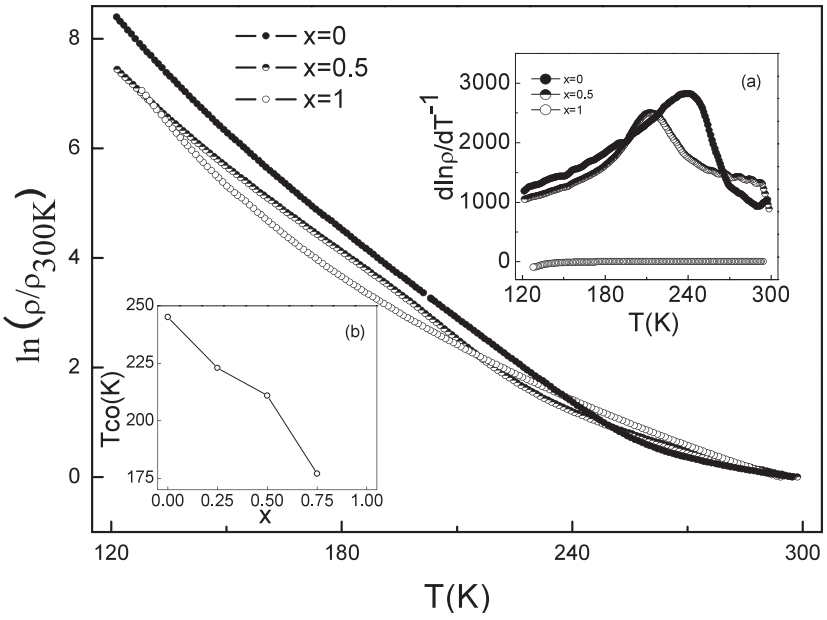

Figure 1. Temperature dependence of the electrical resistance for $(Nd_{0.75}Na_{0.25})_x(Nd_{0.5}Ca_{0.5})_{1-x}MnO_3$ ($x = 0, 0.5, 1$); inset (a): $d\ln\rho/dT^{-1}$ versus T curves corresponding to each sample; inset (b): x dependence of T_{CO} attained by $d(\ln\rho)/d(T^{-1})$.

Table 1. The $\langle r_A\rangle$, σ^2, lattice volume V and lattice parameters for $(Nd_{0.75}Na_{0.25})_x(Nd_{0.5}Ca_{0.5})_{1-x}MnO_3$.

Composition	$\langle r_A\rangle$	σ^2	V	Lattice parameters (Å)		
x	(Å)	(Å^2)	(Å^3)	a	b	c
0	1.172	0.000 07	221.916	5.3563	5.4566	7.5928
0.25	1.174	0.000 35	226.934	5.3962	5.4950	7.6532
0.5	1.177	0.000 62	227.936	5.4042	5.5034	7.6642
0.75	1.180	0.000 87	228.669	5.4105	5.5128	7.6665
1	1.182	0.001 11	228.911	5.4166	5.5140	7.6643

where V_{min} is the minimum sound velocity over the entire temperature range studied. The experiments were made in a closed cycle refrigerator during the warm-up from 15 K to room temperature at the rate of about 0.1 K min^{-1}.

3. Results

The x-ray diffraction patterns of the samples were obtained by powder x-ray diffraction. All samples are of single phase without detectable secondary phase and can be indexed with the orthorhombic structure of space group *Pnma*. Table 1 lists the lattice parameters of the various compositions, values of $\langle r_A\rangle$ based on ionic radii for nine-fold coordination [21], and the size variances σ^2. It can be found that the lattice parameters and lattice volume increase as the Na content increases. That is because the calcium's ionic radius is a little smaller than the sodium's ($r(Na^+) = 1.24$ Å, $r(Ca^{2+}) = 1.18$ Å [21]).

The temperature dependences of the electrical resistivity are shown in figure 1 for some samples ($x = 0, 0.5, 1$). All samples show semiconductor-like transport behaviour in the whole

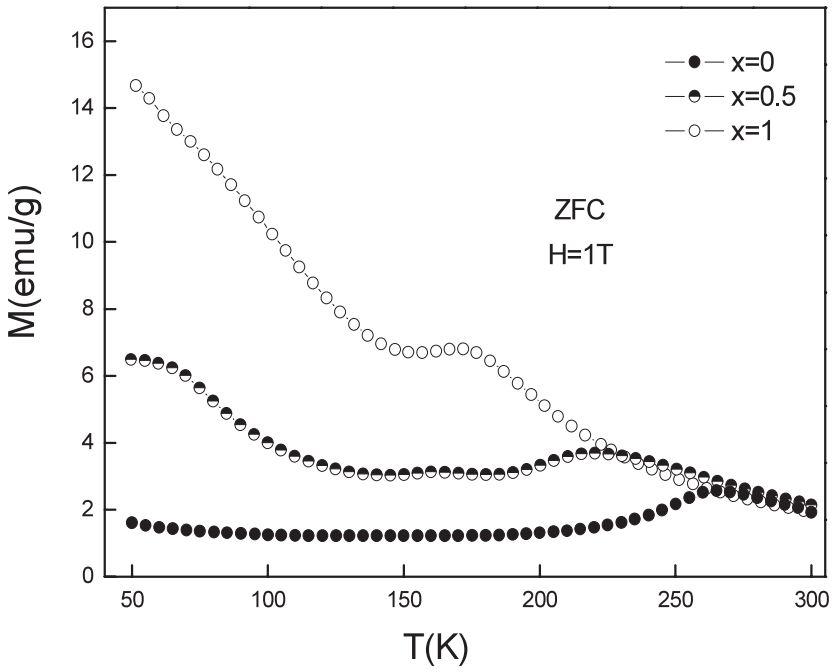

Figure 2. Temperature dependence of the magnetization of $(Nd_{0.75}Na_{0.25})_x(Nd_{0.5}Ca_{0.5})_{1-x}MnO_3$.

temperature range and exhibit a discernible slope change around T_{CO}. The $d(\ln\rho)/d(T^{-1})$ versus T curves are plotted in the inset (a) of figure 1. One can see that except for $x = 1$ all curves show an abnormal peak. Usually T_{CO} is determined by neutron diffraction and not from $d(\ln\rho)/d(T^{-1})$. But it is true that the derivative exhibits a peak close to T_{CO} [22]. So T_{CO} can be estimated through $d(\ln\rho)/d(T^{-1})$–T curves. T_{CO} shifts to lower temperature with increasing x, as shown in inset (b) of figure 1.

The variations of the magnetizations with temperature of the system are shown in figure 2. The zero-field-cooled (ZFC) curves were obtained from 50 to 300 K in an applied magnetic field of 1 T. For $x = 0$, the magnetization first increases as temperature decreases, then reaches a maximum value around $T_{CO} \sim 250$ K. Below 80 K, the magnetization increases with decreasing temperature, which is usually ascribed to the paramagnetic (PM) behaviour of Nd ions [23]. Other samples show similar magnetic behaviours. It can be seen that in the low-temperature range the increases of the magnetization with increasing Na concentration indicate that the ferromagnetism of the system is strengthened.

The temperature dependences of the relative longitudinal ultrasonic velocity and attenuation are shown in figure 3. For $x = 0$, the longitudinal sound velocity show slight softening ($-\Delta V/V \sim -2\%$) associated with a sharp attenuation peak as cooling down from room temperature to T_{P1} which is close to the T_{CO}. Just below T_{P1}, the sound velocity stiffens dramatically. The dramatic ultrasonic sound velocity and attenuation anomalies near T_{CO} result from strong electron–phonon coupling via the Jahn–Teller distortion of the $Mn^{3+}O_6$ octahedron [18–20]. Besides the dramatic sound velocity and attenuation anomalies that occurred near T_{CO}, another attenuation peak was observed at $T_{P2} \sim 100$ K. With increasing x, T_{P1} and the associated attenuation peak shift to lower temperature, while the lower temperature attenuation peak becomes more considerable and shifts to higher temperature until merging with the attenuation peak at high temperature for $Nd_{0.75}Na_{0.25}MnO_3$.

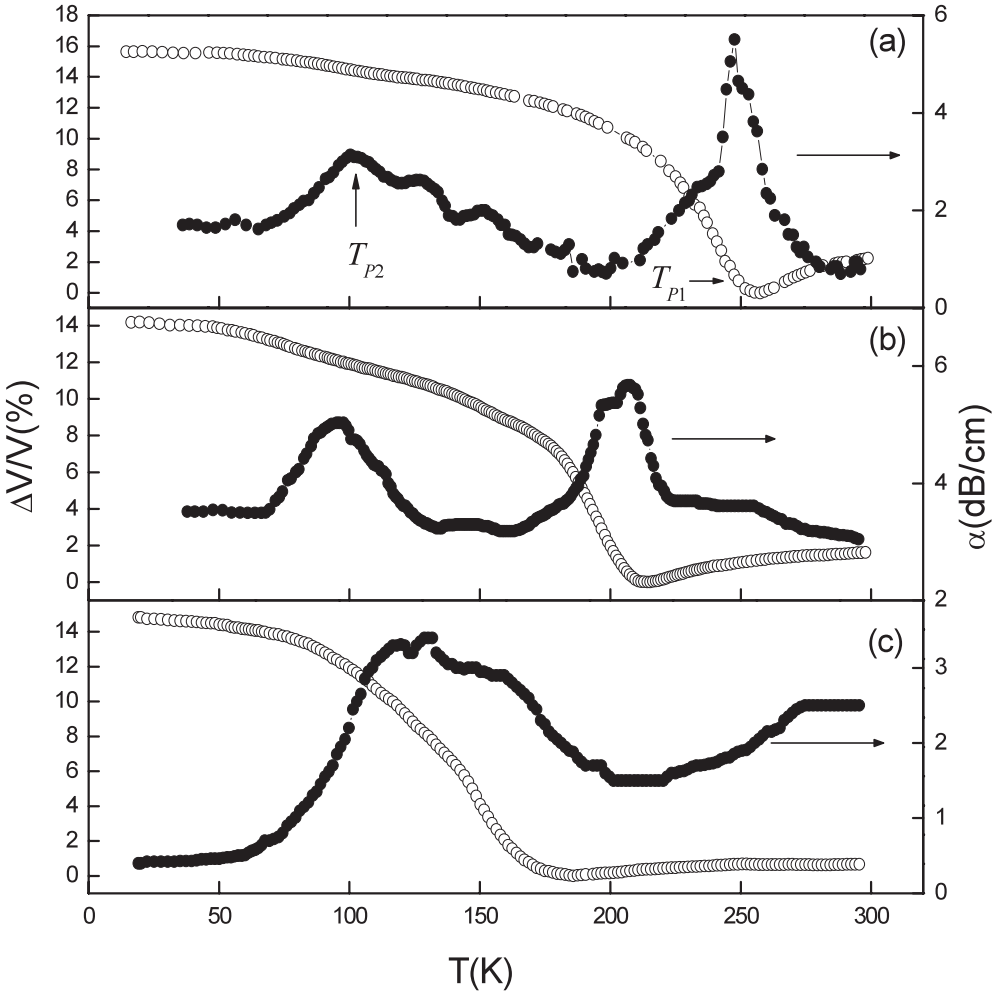

Figure 3. Temperature dependence of the ultrasonic longitudinal sound velocity and attenuation for $(Nd_{0.75}Na_{0.25})_x(Nd_{0.5}Ca_{0.5})_{1-x}MnO_3$: (a) $x = 0$, (b) $x = 0.5$, (c) $x = 1$.

4. Discussion

From the resistivity and magnetization results (see figure 1), one may notice that the charge-ordering transition of $(Nd_{0.75}Na_{0.25})_x(Nd_{0.5}Ca_{0.5})_{1-x}MnO_3$ shifts to lower temperature with increasing x. In the case of $x = 1$, the peak in the $d(\ln\rho)/d(T^{-1})$ versus T curve as a signal of the CO transition no longer shows up. This result shows clearly that the charge ordering becomes weaker and unstable with the substitution of Ca^{2+} by Na^{+} in $(Nd_{0.75}Na_{0.25})_x(Nd_{0.5}Ca_{0.5})_{1-x}MnO_3$. Although the ultrasonic velocity softening also shifts to low temperature as x increases, the ultrasonic anomaly still exists in the sample with $x = 1$ (see figure 3). According to previous reports [18–20], this anomalous velocity change arises from electron–phonon coupling that originates from the Jahn–Teller effect. The absence of a peak in the $d(\ln\rho)/d(T^{-1})$ versus T curve shows that the long-range charge ordering is destroyed, while electron–phonon coupling still exists for $x = 1$, indicating the $Nd_{0.75}Na_{0.25}MnO_3$ may be a short-range charge-ordered system.

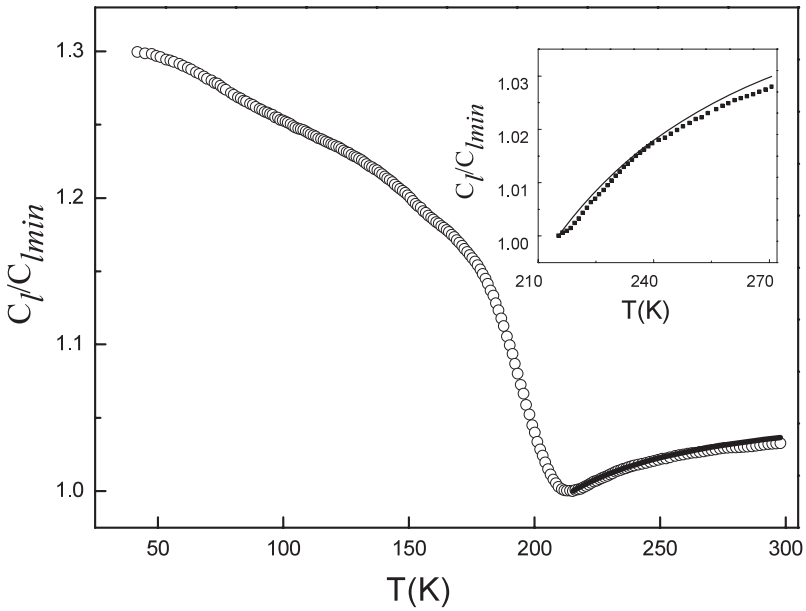

Figure 4. The longitudinal modulus $C_l(T)$ as a function of temperature for $(Nd_{0.75}Na_{0.25})_{0.5}(Nd_{0.5}Ca_{0.5})_{0.5}MnO_3$. Open symbols are experimental data; solid lines are calculated results using equation (2). The inset is an enlarged part of $C_l(T)$ above T_{co}.

According to other studies [5, 9], the stability of the charge ordering can be greatly affected by the $\langle r_A \rangle$ and σ^2. As shown in table 1, $\langle r_A \rangle$ stays nearly constant and the size variance σ^2 is very small, so the $\langle r_A \rangle$ and σ^2 should not be the main reasons for the suppression of charge ordering in $(Nd_{0.75}Na_{0.25})_x(Nd_{0.5}Ca_{0.5})_{1-x}MnO_3$. Considering the anomalous phenomena in the Na^+ doped manganites [14, 17], the charge mismatch effect may have impact on suppressing the charge ordering. The large difference in valence between the rare-earth ions and Na^+ results in the large random-potential fluctuations, leading to the inhomogeneous state mixed of the lower potential region (e_g electron mobilized region) and high potential region (e_g electron localized region) [10, 13, 24], which can induce the ferromagnetic cluster on the AFM (antiferromagnetic)-CO matrix and weaken the CO state. As a result, the ferromagnetism of the system is strengthened in agreement with our magnetization results. With increasing Na content, the charge mismatch effect becomes stronger, resulting in the unstable and short-range CO state.

To probe the relationship between the stability of the charge-ordered state and the cooperative Jahn–Teller effect, the temperature dependence of the longitudinal modulus C_l for $(Nd_{0.75}Na_{0.25})_x(Nd_{0.5}Ca_{0.5})_{1-x}MnO_3$ ($x = 0.5$) is plotted in figure 4. The longitudinal modulus C_l can be described as

$$C_l = DV_l^2 \tag{1}$$

where D is the mass density and V_l is the longitudinal ultrasonic velocity. According to the cooperative Jahn–Teller theory, one can obtain the relationship between the elastic modulus $C_l(T)$ and the temperature T above T_{CO} as follows [25]:

$$C_l(T) = C_0\left(\frac{T - T_c^0}{T - \Theta}\right). \tag{2}$$

The characteristic temperature T_c^0 and Θ can be determined by the fitting of the experimental

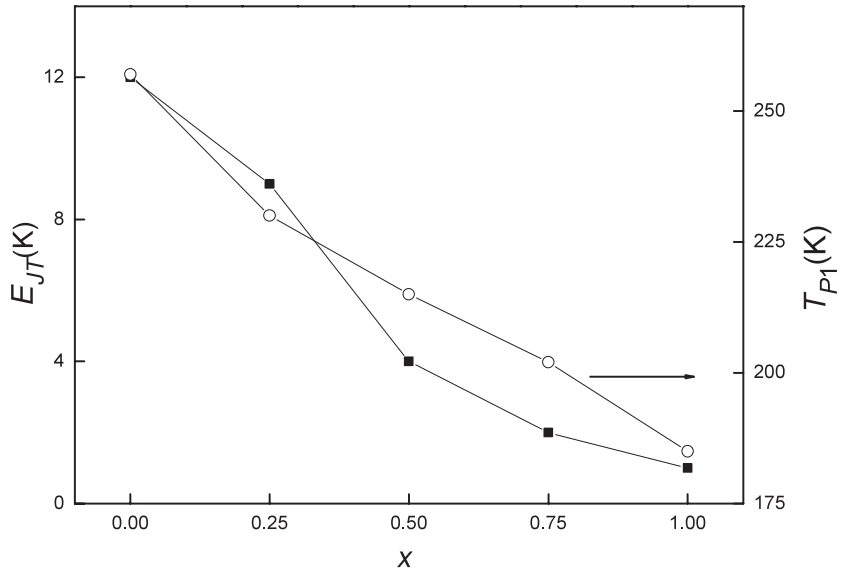

Figure 5. The x dependence of T_{P1} and E_{JT} for $(Nd_{0.75}Na_{0.25})_x(Nd_{0.5}Ca_{0.5})_{1-x}MnO_3$ ($x = 0, 0.25, 0.5, 0.75, 1$).

data around elastic softening. The Jahn–Teller coupling energy E_{JT} which reflects the strength of the cooperative Jahn–Teller coupling is given by $E_{JT} = T_c^0 - \Theta$ [26, 27]. One can clearly see that the fitting results agree well with the experimental data from figure 4, indicating that the cooperative Jahn–Teller effect is the main driving force for charge ordering in $(Nd_{0.75}Na_{0.25})_x(Nd_{0.5}Ca_{0.5})_{1-x}MnO_3$. To quantitatively estimate the strength of the Jahn–Teller coupling, we fitted the longitudinal modulus of all samples by equation (2). The x dependence of T_{P1} attained by the longitudinal ultrasonic velocity measurements and E_{JT} are shown in figure 5. The decrease of E_{JT} and T_{P1} as the Na content increases reflects that the cooperative Jahn–Teller coupling becomes weaker. The analysis of experimental results suggests that the suppression of charge ordering and the weakening of cooperative Jahn–Teller coupling are due to the following effects.

(1) When a rare-earth ion is substituted by a sodium ion, the large valence difference leads to the formation of a Mn^{3+}-rich region and a Mn^{3+}-poor region, which induces the electronic inhomogeneity and ferromagnetic clusters, makes the cooperative Jahn–Teller effect weaker.
(2) Furthermore, the partial substitution of calcium ions with larger sodium ions causes the increase of the average lattice volume (as shown in table 1) and expansion of the MnO_6 octahedron. So the Jahn–Teller active Mn^{3+} can only be frozen at lower temperatures, resulting in a lower charge ordering transition temperature.

Another interesting phenomenon in our experimental results is the attenuation anomaly at low temperature. For $Nd_{0.5}Ca_{0.5}MnO_3$, the anomalous attenuation peak was observed at $T_{P2} \sim 100$ K. From the magnetic curve of $Nd_{0.5}Ca_{0.5}MnO_3$, the increase of magnetization was observed around T_{P2}, which has been ascribed to the PM ordering of Nd ions [23]. So the anomalous attenuation peak at T_{P2} may be attributed to the phase competition of AFM and PM phase for $Nd_{0.5}Ca_{0.5}MnO_3$. As discussed above, the substitution of Ca^{2+} by Na^+ induces the ferromagnetic (FM) cluster on the AFM-CO matrix due to the charge mismatch effect, so the

magnetic phase in the low-temperature range consists of AFM, PM and FM in the Na doped compounds. With increasing x, the charge mismatch effect becomes stronger, which could further weaken the AFM-CO state and induce the FM cluster at higher temperature, so the multiphase competition region is wider. Liu also found that below 130 K there coexists an FM and PM region in $Nd_{0.75}Na_{0.25}MnO_3$ through magnetization and ESR measurements [17]. As a result, the lower-temperature attenuation peak becomes more considerable and moves to higher temperature until merging with the higher-temperature attenuation peak for $Nd_{0.75}Na_{0.25}MnO_3$. The attenuation and magnetization measurements show that the phase competition was intensified due to the charge mismatch effect in $(Nd_{0.75}Na_{0.25})_x(Nd_{0.5}Ca_{0.5})_{1-x}MnO_3$, resulting in the enhancement of phase separation.

5. Conclusion

In summary, we have studied the electrical transport, magnetic and ultrasonic properties of charge-ordered $(Nd_{0.75}Na_{0.25})_x(Nd_{0.5}Ca_{0.5})_{1-x}MnO_3$ perovskite. The ultrasonic anomalies in sound velocity and attenuation near T_{CO} show direct evidence for electron–phonon coupling. At lower temperature, the big attenuation peak indicates the spin–phonon interaction in the compound and provides a trace of phase separation. As the Na content increases, the charge-ordering transition temperature T_{co} shifts to lower temperature, the magnetization of the system is strengthened, and the PS is enhanced. The fitting results of the longitudinal modulus indicate that the charge ordering originates mainly from the cooperative Jahn–Teller lattice distortion and the Jahn–Teller coupling energy E_{JT} becomes smaller with increasing Na doping. From the results, we conclude that: (1) compared with $Nd_{0.5}Ca_{0.5}MnO_3$, $Nd_{0.75}Na_{0.25}MnO_3$ is a short-range charge-ordered system; (2) the charge mismatch effect may play an important role in suppressing charge ordering by affecting the local electronic homogeneity around the rare-earth ion and enhancing the PS through inducing the FM cluster on the matrix.

Acknowledgments

This work was supported by the National Natural Science Foundation of China (No. 10274075) and Specialized Research Fund for the Doctoral Program of Higher Education (No. 20030358056).

References

[1] Von Helmolt R, Wecker J, Holzapfel B, Schultz L and Samwer K 1993 *Phys. Rev. Lett.* **71** 2331
[2] Jin S, Tiefel T H, McCormack M, Fastnacht R A, Ramesh R and Chen L H 1994 *Science* **264** 413
[3] Chahara K, Ohno T, Kasai M and Kozono Y 1993 *Appl. Phys. Lett.* **63** 1990
[4] Gu J Y, Ogale B, Rajeswari M, Venkatesan T, Ramesh R, Radmilovic V, Dahmen U, Thomas G and Noh T W 1998 *Appl. Phys. Lett.* **72** 1113
[5] Arulraj A, Santhosh P N, Srinivasa Gopalant R, Guha A, Raychaudhuri A K, Kumar N and Rao C N R 1998 *J. Phys.: Condens. Matter* **10** 8497
[6] Millange F, de Brion S and Chouteau G 2000 *Phys. Rev.* B **62** 5619
[7] Mori S, Chen C H and Cheong S-W 1998 *Phys. Rev. Lett.* **81** 3972
[8] Rodriguez-Martinez L M and Attfield J P 1996 *Phys. Rev.* B **54** 15622
[9] Terai T, Sasaki T, Kakeshita T, Fukuda T and Saburi T 2000 *Phys. Rev.* B **61** 3488
[10] Itoh M, Shimura T, Yu J D, Hayashi T and Inaguma Y 1995 *Phys. Rev.* B **52** 12522
[11] Shimura T, Hayashi T, Inaguma Y and Itoh M 1996 *J. Solid State Chem.* **124** 250
[12] Wang X L, Kennedy S J, Liu H K and Dou S X 1998 *J. Appl. Phys.* **83** 7177
[13] Rao G H, Sun J R, Bärnerand K and Hamad N 1999 *J. Phys.: Condens. Matter* **11** 1523
[14] Ye S L, Song W H, Dai J M, Wang K Y, Wang S G and Du J J 2001 *J. Appl. Phys.* **90** 2943

[15] Roy S, Guo Y Q, Venkatesh S and Ali N 2001 *J. Phys.: Condens. Matter* **13** 9547
[16] Jiráka Z, Hejtmáneka J, Knížeka K, Maryško M, Pollert E, Dlouhá M, Vratislav S, Kužel R and Hervieu M 2002 *J. Magn. Magn. Mater.* **250** 275
[17] Liu X J, Jiang E Y, Li Z Q, Li B L, Li W R, Yu A and Bai H L 2004 *Physica* B **348** 146
[18] Zhu C F and Zheng R K 2000 *J. Appl. Phys.* **87** 3579
[19] Zheng R K, Zhu C F, Xie J Q and Li X G 2000 *Phys. Rev.* B **63** 024427
[20] Li X G, Zheng R K, Li G, Zhou H D, Huang R X, Xie J Q and Wang Z D 2002 *Europhys. Lett.* **60** 670
[21] Shannon R D 1976 *Acta. Crystallogr.* A **32** 751
[22] Ramirez A P, Schiffer P, Cheong S W, Chen C H, Bao W, Palstra T T M, Gammel P L, Bishop D J and Zegarski B 1996 *Phys. Rev. Lett.* **76** 3188
[23] Millange F, de Brion S and Chouteau G 2000 *Phys. Rev.* B **62** 5619
[24] Coey J M D, Viret M, Ranno L and Ounadjela K 1995 *Phys. Rev. Lett.* **75** 3910
[25] Melcher R L 1976 *Physical Acoustics* vol 12, ed W P Mason and R N Thurston (New York: Academic) pp 1–77
[26] Hazama H, Goto T, Nemoto Y, Tomioka Y, Asamitsu A and Tokura Y 2000 *Phys. Rev.* B **62** 15012
[27] Kugel K I and Khomskii D I 1982 *Usp. Fiz. Nauk* **136** 621
Kugel K I and Khomskii D I 1982 *Sov. Phys.—Usp.* **25** 231 (Engl. Transl.)